

Interpreting a 1 fb^{-1} ATLAS Search in the Minimal Anomaly Mediated Supersymmetry Breaking Model

B.C. Allanach,^a T.J. Khoo,^b K. Sakurai^{a,b,c}

^a*Department of Applied Mathematics and Theoretical Physics, Centre for Mathematical Sciences, University of Cambridge, Wilberforce Road, Cambridge CB3 0WA, United Kingdom*

^b*Department of Physics, Cavendish Laboratory, J J Thomson Avenue, Cambridge, CB3 0HE, United Kingdom*

^c*Department of Physics, Nagoya University, Nagoya 464-8602, Japan*

E-mail: B.C.Allanach@damtp.cam.ac.uk, khoo@hep.phy.cam.ac.uk,
sakurai@hep.phy.cam.ac.uk

ABSTRACT: Recent LHC data significantly extend the exclusion limits for supersymmetric particles, particularly in the jets plus missing transverse momentum channels. The most recent such data have so far been interpreted by the experiment in only two different supersymmetry breaking models: the constrained minimal supersymmetric standard model (CMSSM) and a simplified model with only squarks and gluinos and massless neutralinos. We compare kinematical distributions of supersymmetric signal events predicted by the CMSSM and anomaly mediated supersymmetry breaking (mAMSB) before calculating exclusion limits in mAMSB. We obtain a lower limit of 900 GeV on squark and gluino masses at the 95% confidence level for the equal mass limit, $\tan \beta = 10$ and $\mu > 0$.

KEYWORDS: Supersymmetric Phenomenology, exclusion, Large Hadron Collider

Contents

1	Introduction	1
2	The ATLAS 0-lepton Search	2
3	Our Simulation of the ATLAS Search	4
3.1	Validation of Our Simulation	4
4	mAMSB Simulation	6
4.1	Comparison of Signal Events Between the CMSSM and mAMSB	7
4.2	mAMSB Scan: Properties of SUSY Events	10
4.3	Exclusion Limits in mAMSB	12
4.4	Combination of Signal Regions	13
5	Summary and Conclusions	13

1 Introduction

Initial supersymmetric particle search data from ATLAS [1, 2] and CMS [3] have now been extended from 35 pb^{-1} to 1 fb^{-1} [4–7]. The data, collected from pp collisions at $\sqrt{s} = 7 \text{ TeV}$, feature significant missing transverse momentum and jet activity. Other topologies have also been examined, but in most scenarios of supersymmetry breaking, the jets plus missing transverse momentum signatures are the most sensitive. None of these searches has found a significant signal over the expected Standard Model (SM) background, and so they have set limits on sparticle production. Within the CMSSM [8–13], the strongest limits come from the ATLAS “0-lepton” search [4] which excludes squarks and gluinos with masses below 950 GeV (in the equal mass limit) at 95% C.L. in the $A_0 = 0$, $\tan(\beta) = 10$, $\mu > 0$ slice of the CMSSM, and the CMS hadronic searches that extend the mass limit to 1.1 TeV [5–7]. A limit at this scale was already anticipated in the absence of a signal [14].

The experiments present their CMSSM limits on the scalar-gaugino universal mass (m_0 , $m_{1/2}$) plane for particular values of $\tan \beta$ (the ratio of the two MSSM Higgs vacuum expectation values) and A_0 (a GUT-scale universal tri-linear scalar coupling parameter). Earlier LHC supersymmetry (SUSY) searches based on only 35 pb^{-1} of integrated luminosity have been reinterpreted for different values of A_0 and $\tan \beta$ from those presented by the experiments [15]. The earlier searches were also reinterpreted in terms of gauge mediation and some benchmark SUSY breaking models [16]. Searches based on 165 pb^{-1} have also been investigated in a SUSY breaking model which has certain non-universalities motivated by naturalness in electroweak symmetry breaking [17]. The first fb^{-1} of preliminary LHC data has been used to confront the no-scale $F - SU(5)$ model [18] and, more recently, the

data were published and exclusion limits in the phenomenological MSSM [19] were calculated, combining channels with leptons, jets and missing transverse momentum with the jets plus missing transverse momentum channels. The present paper is in a similar spirit to these earlier works: it is our aim to assess the impact of the most recent published 0-lepton results based on 1 fb^{-1} of integrated luminosity on the mAMSB model [20]. We also wish to study the effectiveness of the experimental cuts in the context of mAMSB. mAMSB is a model worthy of study, since it avoids the flavour and SUSY CP problems [21–23] by introducing the additional universal soft mass m_0 and can provide the correct relic density of dark matter in a natural way in a sequestered hidden sector [24, 25].

ATLAS also presented their exclusion limits in the squark-gluino mass plane [4], assuming all other particles are heavy, except for the the neutralino which is massless. One may ask whether one should just take this simplified model, and apply it to the parameter space of mAMSB. Each point in mAMSB parameter space corresponds to some gluino and squark mass and a light neutralino and so, in principle, one could just chart the approximate exclusion in the mAMSB parameter space without performing any event simulation, instead only calculating the sparticle spectrum. We shall show that this leads to a poor approximation of the 0-lepton search exclusion for the full mAMSB model. Thus, we shall need to simulate sparticle production in mAMSB.

Early work on collider signatures of mAMSB focused on the usual supersymmetric signatures [26] as well as searching for the decays of the lightest charginos into the lightest neutralinos [27]. These two particles being close in mass is a prediction of mAMSB, and the hope was to confirm this by measuring the decays of one into the other. The LHC experiments have so far not yet published results using the special techniques of searching for the lightest chargino decays, and so we do not comment on them further. It was also recently shown that a light CMSSM point containing the “golden” supersymmetric decay cascade chain $\tilde{q} \rightarrow \chi_2^0 \rightarrow \tilde{e}_R \rightarrow \chi_1^0$ could be distinguished against mAMSB on the basis of kinematic end-point measurements alone [28] with just 10 fb^{-1} of LHC data. Unfortunately, such a light CMSSM point has been excluded by the 2011 LHC searches and no sign of the golden chain has been seen.

The paper proceeds as follows: we present the cuts and summarise the results of the ATLAS 0-lepton search in section 2. Next, in section 3, we describe our simulation of the ATLAS search, first validating our simulation against their results in the CMSSM. We then simulate mAMSB signals, putting them through the same analysis in section 4. We investigate the properties of interest of mAMSB signal events and compare them to those of the CMSSM. We then calculate the main result of our paper: the exclusion limit in mAMSB. The comparison with the simplified model approximation is performed, finding it to be a poor approximation to the full mAMSB exclusion. Finally, in section 5, we summarise and conclude the paper.

2 The ATLAS 0-lepton Search

The ATLAS collaboration based its most recent search on *five* sets of cuts on *two* different variables (the effective mass, m_{eff} , [29, 30] and the magnitude of the missing transverse

	≥ 2 jets	≥ 3 jets	≥ 4 jets	≥ 4 jets'	High mass
$p_T(j_1)$	> 130 GeV	> 130 GeV	> 130 GeV	> 130 GeV	> 130 GeV
$p_T(j_2)$	> 40 GeV	> 40 GeV	> 40 GeV	> 40 GeV	> 80 GeV
$p_T(j_3)$	–	> 40 GeV	> 40 GeV	> 40 GeV	> 80 GeV
$p_T(j_4)$	–	–	> 40 GeV	> 40 GeV	> 80 GeV
$ \vec{p}_T^{\text{miss}} $	> 130 GeV	> 130 GeV	> 130 GeV	> 130 GeV	> 130 GeV
$\Delta\phi$	> 0.4	> 0.4	> 0.4	> 0.4	> 0.4
$\vec{p}_T^{\text{miss}}/m_{\text{eff}}$	> 0.3	> 0.25	> 0.25	> 0.25	> 0.2
m_{eff}	> 1000 GeV	> 1000 GeV	> 500 GeV	> 1000 GeV	> 1100 GeV
Observed	58	59	1118	40	18
Background	$62.4 \pm 4.4 \pm 9.3$	$54.9 \pm 3.9 \pm 7.1$	$1015 \pm 41 \pm 144$	$33.9 \pm 2.9 \pm 6.2$	$13.1 \pm 1.9 \pm 2.5$
$\sigma \times A \times \epsilon/\text{fb}$	22	25	429	27	17

Table 1. The cuts used to define the signal regions of the ATLAS-0-lep analysis [4]. $\Delta\phi$ is the minimum azimuthal angle between \vec{p}_T^{miss} and the first three jet p_T s. The jet p_T thresholds, $p_T(j_n)$ are ordered in decreasing order. We also display the number of events ATLAS observed in each region, along with the expected Standard Model backgrounds. The first uncertainty represents the statistical uncertainty on the background, whereas the second labels the systematic uncertainty. In the final row, we show the 95% C.L. exclusion upper limit on the total SUSY cross-section times acceptance times efficiency for each signal region, from Ref. [4].

momentum $|\vec{p}_T^{\text{miss}}|$) which have properties tailored more specifically to the kinematic properties of $\tilde{q}\tilde{q}$, $\tilde{q}\tilde{g}$ and $\tilde{g}\tilde{g}$ production. m_{eff} is defined as the sum of $|\vec{p}_T^{\text{miss}}|$ and the magnitudes of the transverse momentum of the two, three or four highest p_T jets, depending on whether the signal region specifies greater than two, three or four jets, respectively. Alternatively, an *inclusive* m_{eff} variant summing $|\vec{p}_T^{\text{miss}}|$ and the p_T of all jets with $p_T > 40$ GeV is defined for the “high mass” selection requiring four jets with a tighter p_T threshold of 80 GeV.

The cuts defining the search regions used by the ATLAS 0-lepton analysis are given in Tab. 1. Also shown for each signal region are the number of observed events $n_o^{(i)}$ that made it past cuts and the expected SM backgrounds $n_b^{(i)}$ together with their statistical and systematic errors $\sigma_{b, \text{stat}}^{(i)}$ and $\sigma_{b, \text{syst}}^{(i)}$. $\sigma_{b, \text{syst}}^{(i)}$ incorporate various experimental and theoretical uncertainties on the background predictions, notably those due to the jet energy scale and resolution, and uncertainties on Monte Carlo modelling.

ATLAS constructed frequentist exclusion regions in SUSY parameter space using a profile likelihood ratio method, taking into account theoretical and detector systematics. The information from the five signal regions was combined by defining the test statistic of each parameter point to be a likelihood ratio given by the signal region demonstrating the best expected sensitivity to new physics. Results were presented as 95% Confidence Level (C.L.) exclusion regions in the $(m_{\tilde{g}}, m_{\tilde{q}})$ plane for $m_{\chi_1^0} = 0$ and in the $\tan\beta = 10$, $A_0 = 0$, $\mu > 0$ slice of the CMSSM [4].

3 Our Simulation of the ATLAS Search

In order to estimate SUSY exclusions, we must simulate LHC collisions producing SUSY particles, along with their subsequent decays. In order to do this, the sparticle spectrum is produced with `SOFTSUSY3.1.7` [31] in SUSY Les Houches Accord format [32]. We simulate the production and decay of sparticles using `HERWIG++2.5.1` [33], and detector simulation is by `DELPHES1.9` [34] using a modified ATLAS detector card. Simulating only squark and gluino production for the CMSSM is sufficient, since direct production of neutralinos, charginos or sleptons is negligible. However, in mAMSB, the direct associated production of squarks/gluinos with charginos or neutralinos is significant, and we include these channels in our mAMSB simulation. Jets are defined using the anti- k_T algorithm with $\Delta R = 0.4$ and an energy recombination scheme in `FASTJET2.4.3` [35, 36]. The total SUSY production cross-sections are computed at next-to-leading order in `PROSPINO 2.1` [37]. For each point in parameter space, we simulate 10000 SUSY events in order to deduce expectations for signal yields and kinematic properties. We shall see below that the efficiencies we obtain are typically higher than 10% in each different signal region, meaning that statistical fluctuations in our expected signal yield are negligible.

The ATLAS analysis cuts detailed in Tab. 1 do not include the details of a correction for data corrupted by the loss of some calorimeter regions in ATLAS during part of the data-taking period. To approximate the impact of this additional event cleaning, we apply an estimated correction factor of $A = 0.85$ to the signal acceptance.

As ATLAS computes the limits on the CMSSM parameter space by using a sophisticated likelihood function to run hypothesis tests, it is unfeasible to reinvent their statistical methods without access to the finer details of their signal and backgrounds. Instead, we estimate the exclusion reach of the selection by comparing with ATLAS’ quoted model-independent limits on $(\sigma \times A \times \epsilon)$ for each signal selection shown in Table 1. A model point is considered to be excluded if the value we compute for $(\sigma \times A \times \epsilon)$ exceeds the limits produced by ATLAS. In this way, we take into account the full power of ATLAS’ statistical infrastructure, except for the impact of signal systematics on the limit, which we model as specified below.

The assumptions and approximations we have made in reproducing ATLAS’ analysis are tested as detailed in the next section.

3.1 Validation of Our Simulation

We cannot match the accuracy of ATLAS’ exclusion in parameter space, because we do not have access to a detailed detector simulation. We do perform a more approximate detector simulation with `DELPHES1.9`, but it is important for us to validate this approximation in order to find out how good it is. Importantly, we do not calculate signal systematic errors explicitly in our initial determination: this is impossible for us to do because we are using the quoted ATLAS bounds on $\sigma \times \epsilon \times A$, which also do not include such systematic errors¹. However, in the exclusion contours, ATLAS does determine and include the signal systematic. The signal systematic errors come from uncertainties in the parton density and from

¹Systematic errors upon the background are included, however.

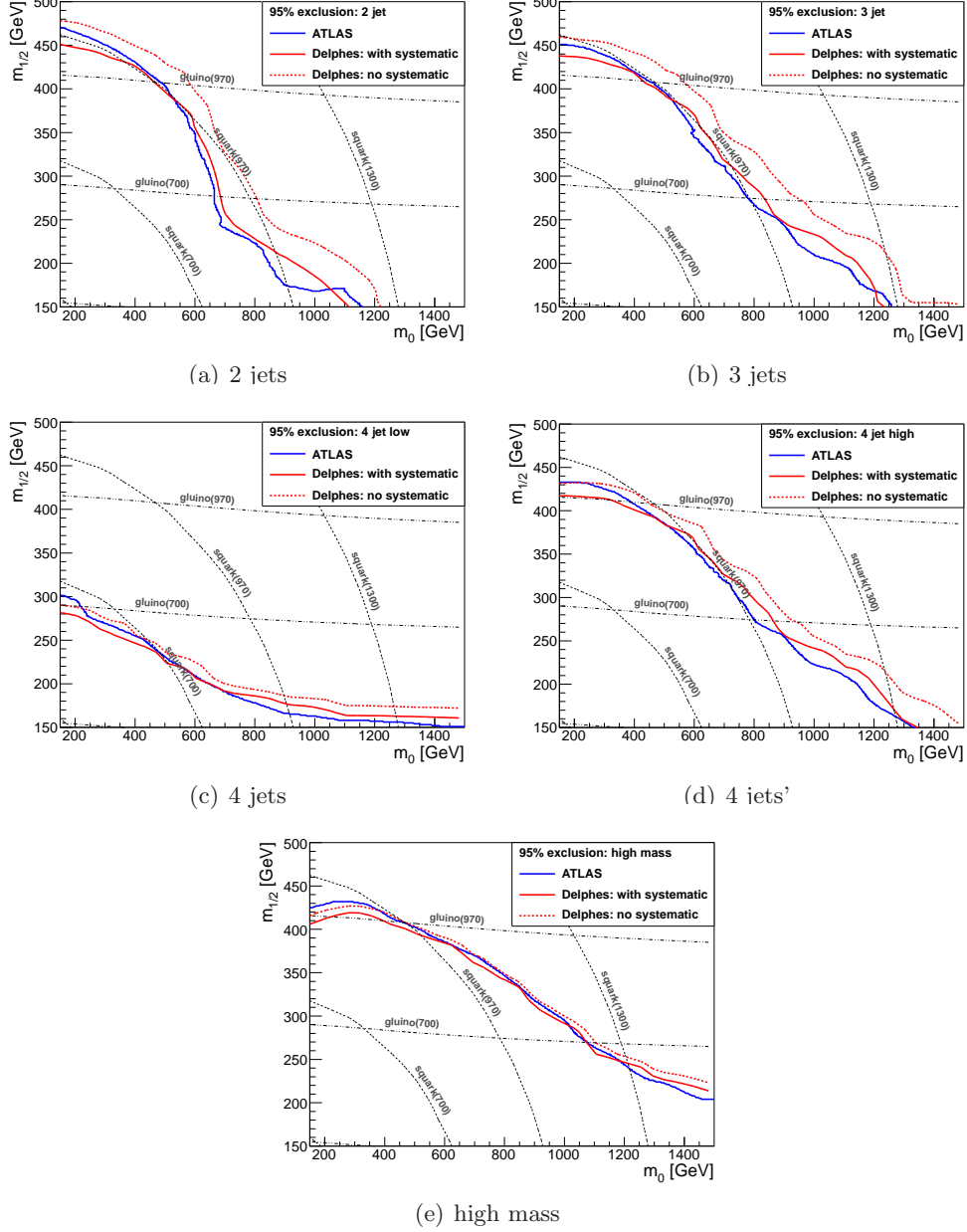


Figure 1. Comparison of our 95% C.L. exclusion limits with those of ATLAS in the case of the CMSSM with $\tan\beta = 10$, $A_0 = 0$ and $\mu > 0$. Each sub-figure shows a different signal region, as defined in Table 1. One solid curve shows our estimate including signal systematic errors, the other shows ATLAS’ [4]. The dashed curve shows our estimate neglecting systematic errors in the signal. We show iso-contours of gluino and squark mass as labelled dotted lines.

higher order corrections and from uncertainties due to initial state radiation modelling and other jet modelling and measurement effects. If we had enough information to reconstruct the likelihood, we could make an attempt to calculate some components of the systematic error. Instead, we here perform a rough ‘by eye’ fit, allowing a different systematic error

for each signal region that does not depend on the SUSY breaking parameters. The systematic error in the likelihood changes ϵ by a factor of s_R for each signal region R . We then estimate a measured cross-section of $\sigma \times \epsilon \times A \times s_R$ for each signal region R .

We now present the validation of our determination of the exclusion by comparing our approximation with that of ATLAS' in the case of the CMSSM. ATLAS determined the exclusion for $\tan\beta = 10$, $A_0 = 0$ and $\mu > 0$ in the CMSSM [4]. We use ATLAS' quoted 95% C.L. bounds on $\sigma \times A \times \epsilon$, where we calculate ϵ from our simulation and σ from PROSPINO 2.1 [37], displaying the contour as a solid line in Fig. 1, where we have included the systematic error in each signal region as stated above. We find that signal systematic error factors of $s_{2j} = s_{3j} = 0.7$, $s_{4j} = s_{4j'} = 0.8$ and $s_{hm} = 0.9$ reproduce the ATLAS exclusion contours quite well, as the figure shows. Our determination of the exclusion contours *neglecting* systematic error is shown as the dashed contours. These clearly are a worse approximation. In the equal squark-gluino mass limit, and using our approximate exclusion limits, we obtain a lower bound on the mass of 970 GeV at 95% CL from Fig. 1a². This combined exclusion limit is defined by using the most restrictive signal region at the parameter point in question. For the equal squark-gluino mass limit, the most sensitive region is the 2 jets region. We see that at this point, the ATLAS exclusion lays on top of our exclusion. However, ATLAS quotes an equivalent bound of 950 GeV, close but different to our determination. This 20 GeV difference is due to the different SUSY spectrum generators used: whereas SOFTSUSY3.1.7 is used here, ATLAS used ISASUSY7.80 [38]. Such differences are caused by higher order corrections in the respective calculations, and as such form part of the theoretical error [39]. By examining the difference between the ATLAS exclusion limits and our estimate, we estimate an error in our exclusion of around 30 GeV in the squark and gluino masses. We see that the signal regions which are most sensitive are the 2-jet search region at high $m_{1/2}$ and low m_0 , and the high mass region at large m_0 and low $m_{1/2}$. In each signal region, our estimate of the exclusion is similar to that of ATLAS, and we conclude that our approximation is reasonable. We should therefore be able to re-simulate signal events in different supersymmetry breaking scenarios in order to evaluate exclusion limits upon them. We now perform this task in mAMSB.

4 mAMSB Simulation

We now simulate the SUSY signals for a grid of mAMSB points for $\tan\beta = 10$ and $\mu > 0$ in mAMSB, applying the ATLAS cuts to them as we did for the CMSSM, above and using the signal systematic errors as determined in our validation, section 3.1. In mAMSB, we scan over m_0 and $m_{3/2}$, the auxiliary mass, which the AMSB soft SUSY breaking terms are proportional to (for further details on the connection between these parameters and the SUSY spectrum, see Ref. [21]). In practice, limited mainly by disk storage (since the event files are very large), we scan in an 11 by 11 grid.

To get a sense of the mAMSB model characteristics, we plot some relevant mass parameters across the parameter plane in Fig. 2. The gluino and squark mass variation is

²If we were to use the zero signal-systematic contours, we would obtain a badly determined bound of 1020 GeV.

similar to that shown by the CMSSM. Between the chargino next-to-lightest supersymmetric particle (NLSP) and neutralino lightest supersymmetric particle (LSP), there is only a small mass gap of a few hundred MeV, which is also illustrated in Fig. 2.

The SUSY signal generation is restricted to processes producing at least one strongly-interacting sparticle. This is to ensure that the events are not dominated by the production of two LSPs or NLSPs, as such events are effectively invisible. As long as the squark and gluino masses are relatively low, i.e. below a TeV, strong production dominates the remaining SUSY cross-section. Above this mass scale, the production shifts towards electroweak associated production of one gaugino and one squark or gluino. This potentially impacts on the efficiency of the signal selection as the mass scale grows, although heavy sparticles are typically quite visible due to the fixed and large mass-splittings.

The largest direct production total SUSY cross-section at the mAMSB point is $\tilde{g}\chi_1^\pm$ production at 11 fb, but many other processes are important, for instance $\tilde{g}\tilde{u}_L$ production at 10 fb. At the CMSSM point, the largest SUSY direct production cross-sections are $\tilde{g}\tilde{u}_R$ production at 9 fb, $\tilde{g}\tilde{u}_L$ production at 7 fb and $\tilde{u}_L\tilde{d}_L$ production at 6 fb. Direct squark/gluino production in association with a weak-ino is important at the mAMSB point (in contrast with the CMSSM). Fig. 3 illustrates the variation of the fraction of electroweak associated production over the total SUSY cross-section generated. At large m_0 and large $m_{3/2}$, the cross-section is entirely due to associated production.

4.1 Comparison of Signal Events Between the CMSSM and mAMSB

For a fair comparison, we pick two points with very similar mass spectra, specifically ($m_0 = 384$ GeV, $m_{3/2} = 44$ TeV) in the mAMSB case and ($m_0 = 455$ GeV, $m_{1/2} = 420$ GeV) from the CMSSM. These points have degenerate squark and gluino masses of about 980 GeV, lying near the border of the 95% ATLAS CMSSM exclusion limit in the equal squark-gluino mass limit. We display the two points' spectra and most likely decays in Fig. 4. In the figure, the quasi-degenerate lightest neutralino and lightest chargino are evident for the mAMSB point.

We now turn to the characteristic lightest chargino decays in mAMSB. In our simulated sample mAMSB point, 6002 lightest charginos were produced, out of 10000 SUSY events. Of these, 24 decayed into a muon, 138 into an electron and the rest into charged pions. We show the p_T distribution of all lightest chargino decay products in Fig. 5. The figure shows that all visible decay products have $p_T < 2$ GeV; the LSP typically carries virtually all the momentum from the lightest chargino. The SM decay products are difficult to distinguish from other soft particles produced in LHC events, and would certainly require a dedicated analysis such as the one in Ref. [27] in order to verify that they come from the lightest chargino decay. For an analysis such as ours, these decays are effectively invisible. However, hard leptons are available from other decay chains. For instance, because the sleptons are between the χ_2^0 and χ_1^0 masses in the mAMSB point, decays through the χ_2^0 will more often lead to hard leptons, violating the lepton veto and leading to less efficiency than in the CMSSM point for the zero leptons channel.

To illustrate the similarities and differences in the mAMSB and CMSSM models, we compare a selection of relevant kinematic variables in Fig. 6. We wish to see if the ATLAS

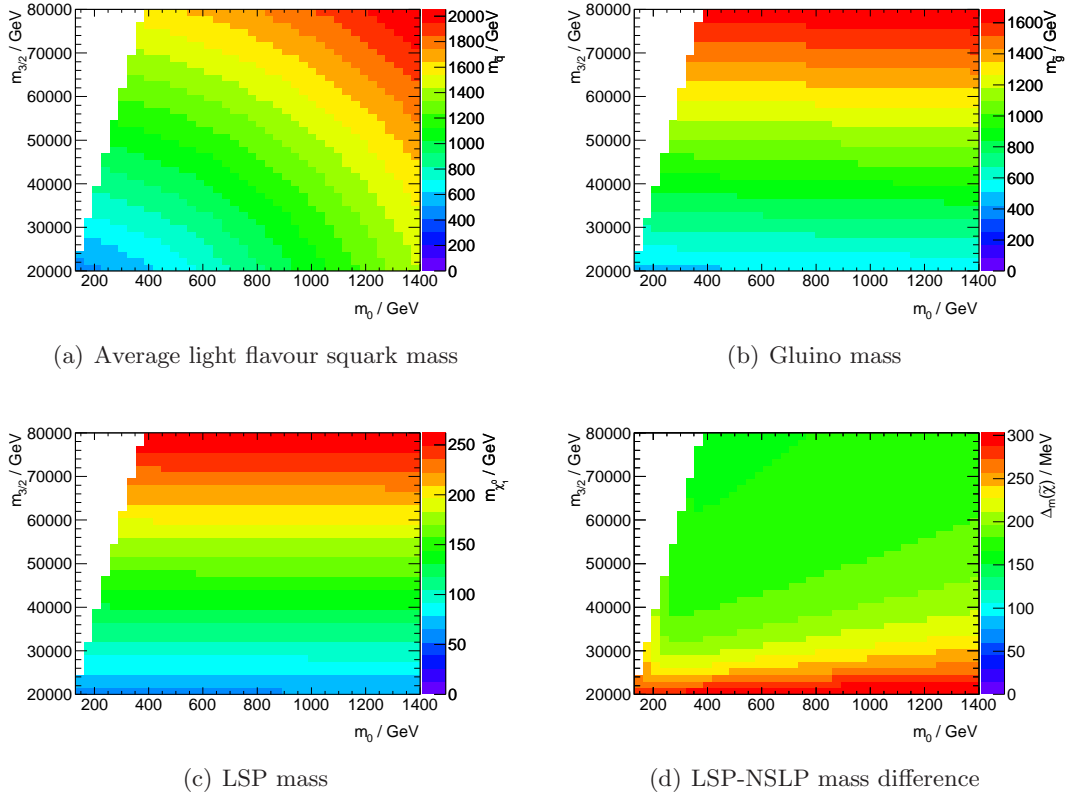


Figure 2. Masses of the squarks, gluinos and LSP (a-c) and the mass-splitting between the LSP and chargino NLSP (d) across the mAMSB $m_0 - m_{3/2}$ plane for $\tan\beta = 10$ and $\mu > 0$. The white region in the top left of each plot is theoretically excluded due to the presence of negative mass-squared scalars.

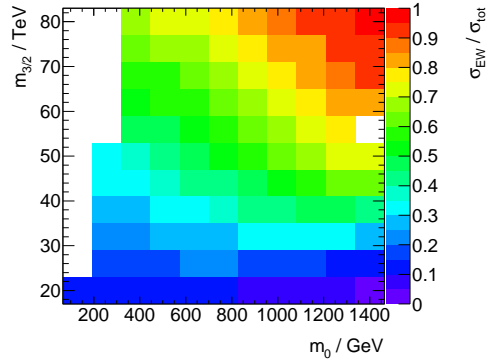
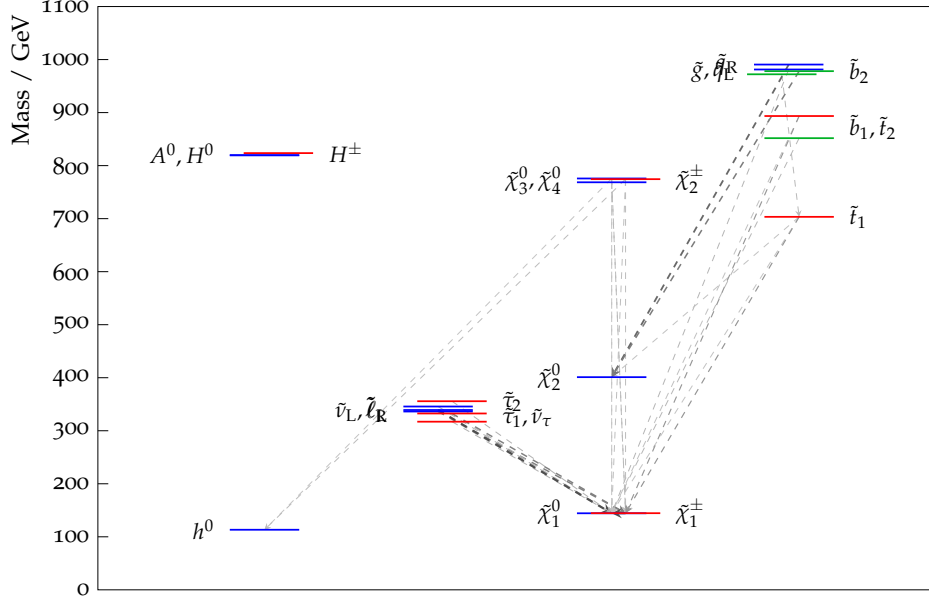
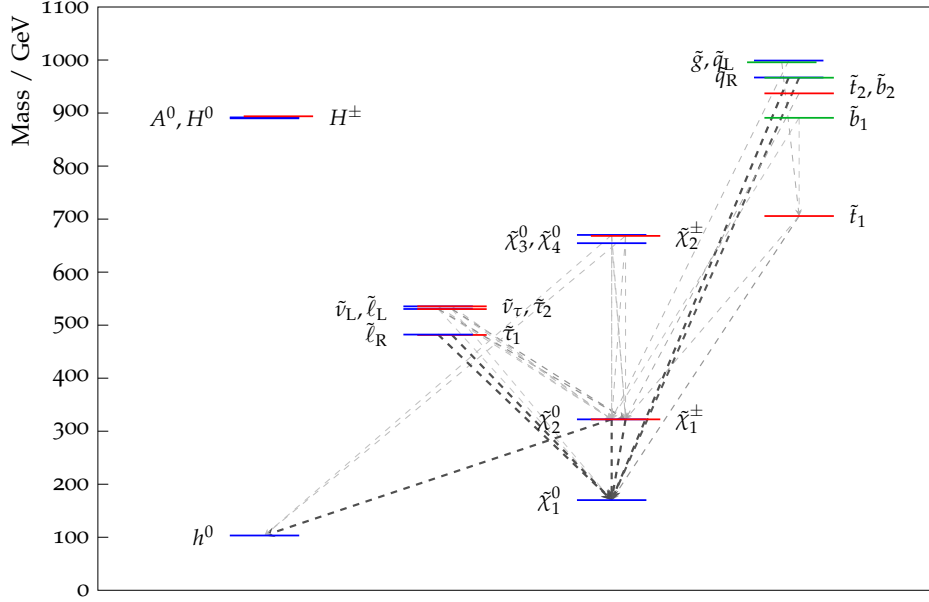


Figure 3. Variation across the mAMSB $m_0 - m_{3/2}$ plane of the fraction of electroweak production over the total SUSY production cross-section, requiring at least one squark or gluino to be produced. The white region in the top left of each plot is theoretically excluded due to the presence of negative mass-squared scalars, while the white spot on the right is due to a failed MC job.



(a) mAMSB point



(b) CMSSM point

Figure 4. Spectra and decays of the mAMSB and CMSSM model points studied. Only decays whose branching ratios are higher than 20% are shown by the arrows. Both points have $\tan \beta = 10$, $\mu > 0$. For the mAMSB point, we have $m_0 = 384$ GeV and $m_{3/2} = 44$ TeV, whereas the CMSSM point has $m_0 = 455$, $m_{1/2} = 420$ and $A_0 = 0$.

selections are efficient for mAMSB, or whether the distributions suggest radically different cuts. No *a priori* kinematic selection is applied to these events, apart from the basic object selections needed to conform with ATLAS variable definitions, such as requiring each jet

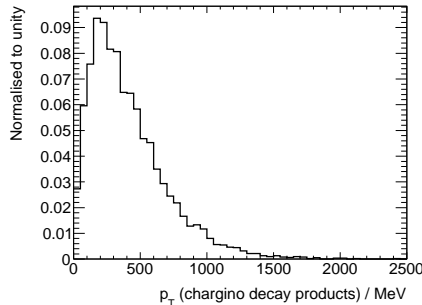


Figure 5. p_T spectrum of visible lightest chargino decay products in mAMSB, for $m_0 = 384$ GeV, $m_{3/2} = 44$ TeV, $\tan\beta = 10$ and $\mu > 0$. No detector simulation or kinematic selection is applied.

used in the m_{eff} computation to have 40 GeV in p_T .

It is seen that the kinematics of the two model points are reasonably similar. For example, the \vec{p}_T^{miss} distributions of the two models look remarkably similar, making the \vec{p}_T^{miss} cut approximately equally efficient in each case. However, compared to the CMSSM point, the mAMSB point has less jets, the hardest jet is softer on average and m_{eff} is smaller. These all make the corresponding cuts somewhat *less efficient* in the case of mAMSB as compared to the CMSSM. The cuts on $\vec{p}_T^{\text{miss}}/m_{\text{eff}}$ are *more efficient* for the mAMSB point, but in fact this effect is swamped by the less efficient cuts on jets and from the lepton veto. We also see that M_{T2} tends to be smaller for the mAMSB point because of the softer jets [40–42]. Although this variable is not used in the present search, it has similar search power to other methods, but in some cases can discover generic MSSM parameter points when the usual m_{eff} , \vec{p}_T^{miss} searches cannot [43]. We therefore advocate its inclusion as part of the searches, even though a lower cut of a few hundred GeV looks to be slightly more efficient for the CMSSM model point than the mAMSB model point examined.

We may understand these kinematic differences as follows: the sparticle cascade decay chains starting from gluinos or squarks, feature decays through lightest charginos prominently in both the CMSSM and mAMSB points. In mAMSB, the lightest charginos are invisible to our analysis as explained above, whereas at the CMSSM point, they decay to $W\chi_1^0$, so the W leads to additional jets (any that decay leptonically are likely to be vetoed), contributing to the jet multiplicity and m_{eff} . A softer m_{eff} for mAMSB then leads to a more highly peaked $m_{\text{eff}}/\vec{p}_T^{\text{miss}}$ ratio. There is also a larger cross-section for weak gaugino/strongly interacting SUSY particle production in mAMSB, making m_{eff} softer. More of the squarks decay through χ_2^0 in mAMSB compared to CMSSM, and since it is heavier, this reduces the p_T of the (typically hardest) jet involved in the decay.

4.2 mAMSB Scan: Properties of SUSY Events

We show the fractions of events with 0, 1 and 2 leptons across the mAMSB parameter space in Fig. 7. The isolated lepton veto in the zero lepton search does not cut much of the SUSY signal over much of the parameter space. On the other hand, searches based on

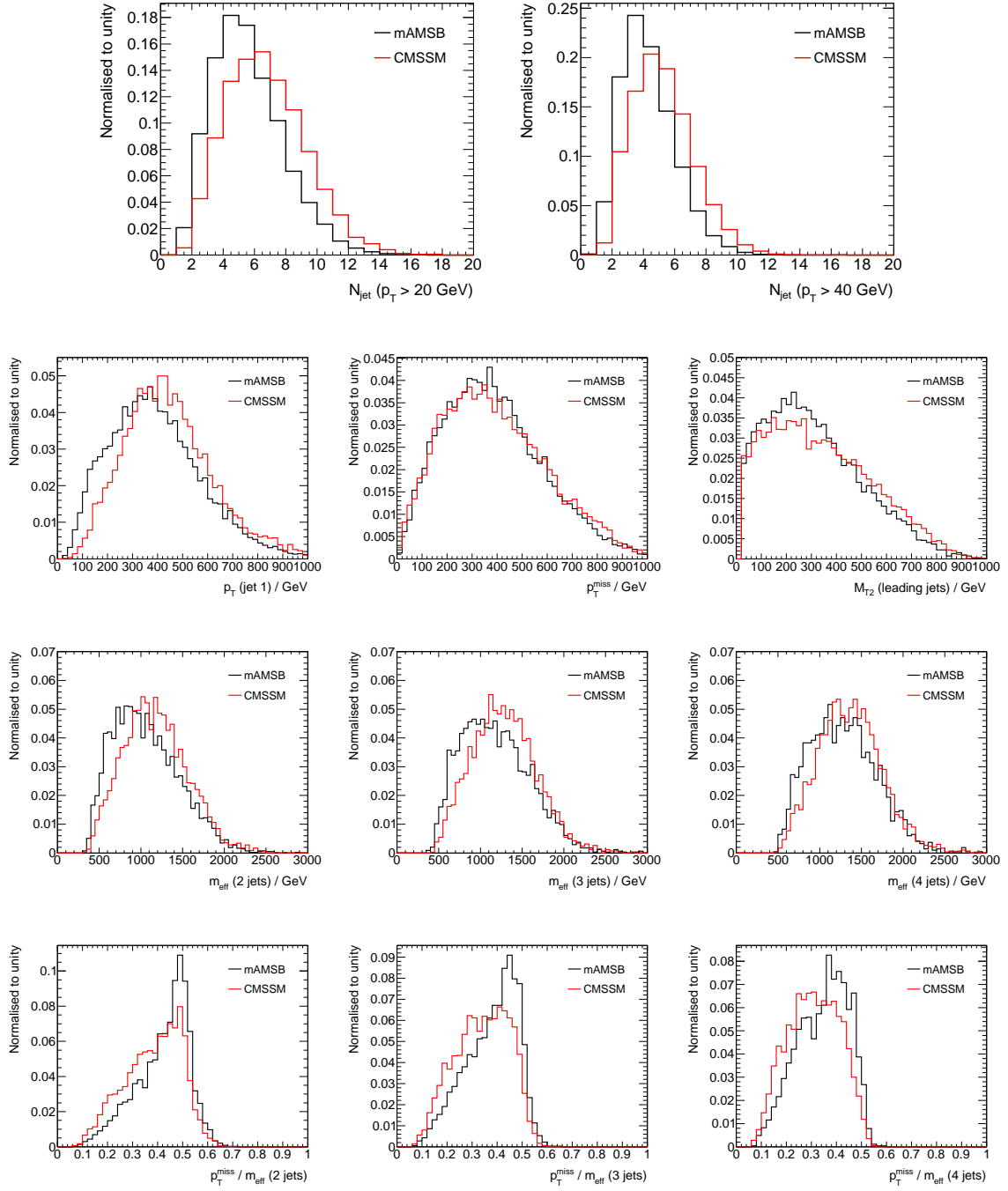


Figure 6. Important kinematic distributions of the signals for mAMSB and CMSSM sample model points for $\tan\beta = 10$ and $\mu > 0$. For the mAMSB point, we have $m_0 = 384$ GeV and $m_{3/2} = 44$ TeV, whereas the CMSSM point has $m_0 = 455$, $m_{1/2} = 420$ and $A_0 = 0$. Only minimal kinematic cuts are applied, i.e. requiring two, three or four jets with $p_T > 40$ GeV for the m_{eff} and $p_T^{\text{miss}}/m_{\text{eff}}$ distributions, as is appropriate.

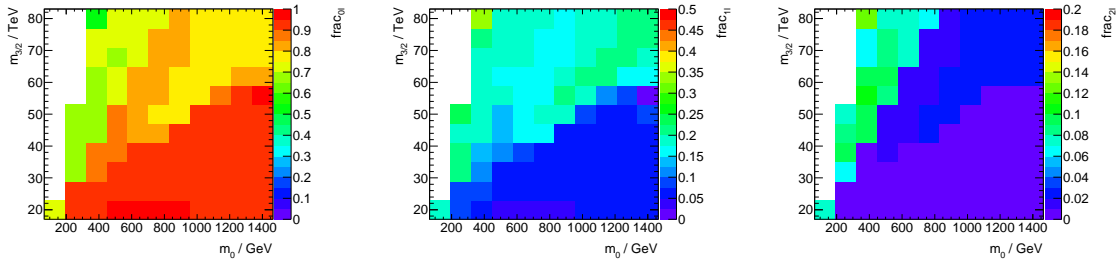


Figure 7. Fraction of events with 0, 1 or 2 hard isolated leptons in the mAMSB parameter space considered in this paper: $\tan\beta = 10$, $\mu > 0$. Leptons with $p_T > 20$ GeV are considered to be hard and isolated if they are not inside a jet (also with $p_T > 20$ GeV). No additional kinematic selection is applied. Note the different z-axis scales in the three plots.

a 1-lepton channel could also be worthy of study, since over roughly half of the parameter space, over 15% of SUSY events have a hard lepton. We show the efficiency of each signal region in the ATLAS 0-lepton search for mAMSB in Fig 8. The ATLAS selections are seen to be reasonably efficient, particularly at greater values of $m_{3/2}$, with the exception of a diagonal strip in which the propensity for producing leptons is greater, as shown in Fig. 7b. The ATLAS signal yields at 1.04 fb^{-1} are plotted in Fig. 9 for each signal region. These values are used to compute the exclusion limits on mAMSB. We see that the parameter space we have chosen has roughly the right range of signal yields expected: naïvely, in the absence of a signal, we would expect the regions with tens of events at the bottom of each plot to be excluded, whereas regions with only one or less expected signal events should evade exclusion.

4.3 Exclusion Limits in mAMSB

We show the 95% confidence level excluded regions for each signal region on the $m_{3/2} - m_0$ parameter space in Fig. 10. We have used the same systematic errors for each signal region as found in the CMSSM search in section 3.1. This is another approximation: any variation of signal systematics between the CMSSM and mAMSB is neglected. We expect this approximation to be good because we obtained a reasonable CMSSM 95% exclusion limit across the parameter space, where the sparticle masses are widely varying. The most sensitive search regions in mAMSB are the 2-jet region at low m_0 and high $m_{3/2}$ and the high mass region at large m_0 . These are the same two regions that are found to be the most sensitive in the CMSSM. In the figure, we display a coloured asterisk which labels which signal region is expected to be the most sensitive at each of our parameter space grid points. We see that near the exclusion contour, for low m_0 the 2-jet region is expected to be most sensitive, then for intermediate $m_0 \sim 500$ GeV, the 4-jet high mass region is, and for $m_0 > 600$ GeV, the high mass region is expected to be the most sensitive.

4.4 Combination of Signal Regions

We combine the excluded regions shown in Fig. 10 to produce a single limit contour on the $m_0 - m_{3/2}$ plane. In principle, such a combination ought to be carried out independently of the data used to set limits, e.g. by following ATLAS’ procedure of excluding based on the best *expected* sensitivity of each signal region. As can be seen in Fig. 10, this statistically correct procedure is approximated in the vicinity of the 95% exclusion contour by taking the union of the excluded regions. This approximation sacrifices perfect frequentist coverage at the point where the different most sensitive signal regions cross, in between our grid points (admittedly, perfect coverage is already abandoned by the use of the CL_s convention [45]). As ATLAS observes no significant fluctuations away from the background-only expectation, our simplified statistical combination (SSC) should deviate only slightly from the ideal coverage. Thus, the SSC should be unobjectionable to all but the most discerning of frequentist statisticians and US Congresspersons. Experimental collaborations could prevent such abuses as these by including additional information (i.e. the expected model-independent limits) in future results. The combined 95% CL exclusion limit thus calculated is shown in Fig. 11, and is the focal result of our work. We also plot on the figure, the approximate exclusion one would obtain if one naively took the ATLAS 0 lepton simplified model results, in which the only sparticles are gluinos, squarks and a massless neutralino [46]. The region underneath the curve is excluded to 95% confidence, in the CL_s scheme. The trajectory of this curve has squark and gluino masses on the 95% confidence level contour in the simplified model interpretation of the 0-lepton results [4]. We see that over most of the plane, the simplified model *over estimates* the search reach. This is because the simplified model assumes 100% branching ratios into jets, whereas mAMSB has decays into leptons, reducing the efficiency. Overall, we see that a naive interpretation of the simplified models would give a poor approximation to the exclusion³.

When phrased in terms of squark and gluino masses, mAMSB is *less* constrained than the CMSSM. This is due to less efficient kinematic cuts, as described in Section 4.1. The two most important effects are the lepton veto (18% less efficient in our test mAMSB model than the CMSSM model) and a softer m_{eff} distribution in mAMSB (30% less efficient in the mAMSB test model for the most sensitive signal region). We also display the mAMSB1 benchmark line and points mAMSB1.N (N from 1 to 5, increasing upwards) from Ref. [44] in the figure. It is clear that the 1 fb^{-1} data already rule out the first point mAMSB1.1 to 95% C.L., leaving mAMSB1.2 as the next lightest non-excluded point for study.

5 Summary and Conclusions

Recent LHC searches in 1 fb^{-1} of integrated luminosity in the jets, missing transverse momentum and no leptons channel have seen no evidence for supersymmetry. These data have been interpreted by the experiments in terms of the CMSSM and simplified models only. Here, we interpret the data in terms of an exclusion on the parameter space of

³Nevertheless, it gives a rough ball-park estimate, and covers other models than our particular constrained one.

mAMSB. We also investigate the mAMSB signals, comparing to the CMSSM in order to see how different or similar the signal events are expected to be. We also wish to examine how different the exclusion is when phrased in, for example the squark and gluino masses. In fact, mAMSB and the CMSSM have rather similar signal events, although there is some difference in jet multiplicities and $\bar{p}_T^{\text{miss}}/m_{\text{eff}}$. The ATLAS 0-lepton cuts involving the latter ratio are slightly more efficient for our mAMSB test model than for the CMSSM one. Because the SUSY events are so similar, there is no reason to radically change the cuts in the ATLAS selection. The very recent CMS results [5–7] are slightly more constraining than those from ATLAS [4] in certain regions of the CMSSM parameter space, and so their inclusion to provide combined search limits will be an interesting exercise for the future.

We display our summary 95% C.L. exclusion contour in Fig. 11, which is the focal result of this paper. The final combined 95% C.L. exclusion limit in mAMSB, at the equal squark-gluino mass limit, is 900 GeV: a little smaller than 950 GeV in the CMSSM. Our determination should be accurate to around 30 GeV; a more accurate determination would require a dedicated ATLAS analysis, which we heartily advocate.

Acknowledgments

This work has been partially supported by STFC. BCA thanks the IPPP for an associateship. TJK is supported by a Dr. Herchel Smith Fellowship from Williams College. KS is supported in part by YLC (Young Leaders Cultivation) program in Nagoya University. We thank A Barr and the Cambridge SUSY working group for discussions and P Richardson and D Grellscheid for their help in massaging HERWIG++ to accept mAMSB input.

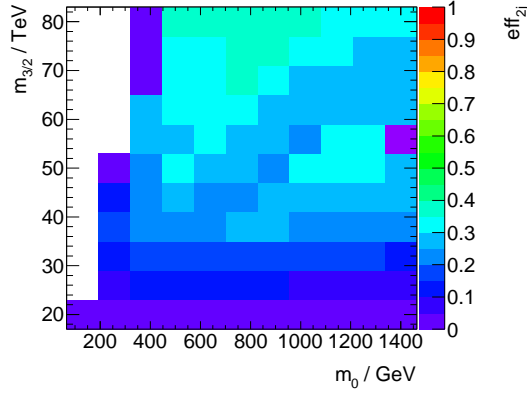
References

- [1] **ATLAS** Collaboration, G. Aad *et. al.*, *Search for squarks and gluinos using final states with jets and missing transverse momentum with the ATLAS detector in $\sqrt{s} = 7$ TeV proton-proton collisions*, [1102.5290](#).
- [2] **ATLAS** Collaboration, G. Aad *et. al.*, *Search for supersymmetry using final states with one lepton, jets, and missing transverse momentum with the ATLAS detector in $\sqrt{s} = 7$ TeV pp* , [1102.2357](#).
- [3] **CMS** Collaboration, V. Khachatryan *et. al.*, *Search for Supersymmetry in pp Collisions at 7 TeV in Events with Jets and Missing Transverse Energy*, [1101.1628](#).
- [4] **ATLAS** Collaboration, G. Aad *et. al.*, *Search for squarks and gluinos using final states with jets and missing transverse momentum with the ATLAS detector in $\sqrt{s} = 7$ TeV proton-proton collisions*, [1109.6572](#).
- [5] **CMS** Collaboration, V. Khachatryan *et. al.*, *Search for Supersymmetry at the LHC in Events with Jets and Missing Transverse Energy*, [1109.2352](#). * Temporary entry *.
- [6] **CMS** Collaboration, V. Khachatryan *et. al.*, *Search for supersymmetry in all-hadronic final states using m_{T_2} in 7 TeV pp collisions at the LHC*, . [CMS-PAS-SUS-11-005](#), * Temporary entry *.

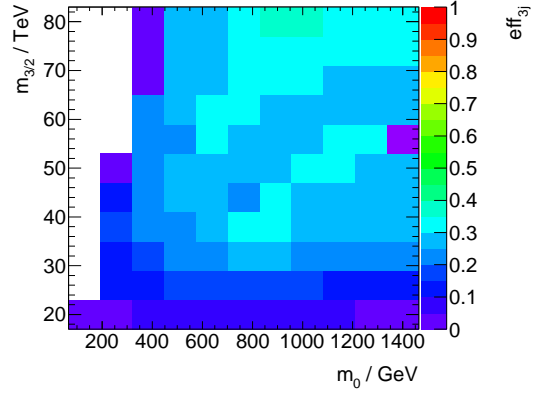
- [7] **CMS** Collaboration, V. Khachatryan *et. al.*, *Search for supersymmetry in all-hadronic events with missing energy*, . [CMS-PAS-SUS-11-004](#), * Temporary entry *.
- [8] A. H. Chamseddine *et. al.*, *Locally Supersymmetric Grand Unification*, *Phys.Rev.Lett.* **49** (1982) 970.
- [9] R. Barbieri, S. Ferrara, and C. A. Savoy, *Gauge Models with Spontaneously Broken Local Supersymmetry*, *Phys. Lett.* **B119** (1982) 343.
- [10] L. E. Ibanez, *Locally Supersymmetric SU(5) Grand Unification*, *Phys.Lett.* **B118** (1982) 73.
- [11] L. J. Hall, J. D. Lykken, and S. Weinberg, *Supergravity as the Messenger of Supersymmetry Breaking*, *Phys.Rev.* **D27** (1983) 2359–2378.
- [12] N. Ohta, *Grand unified theories based on local supersymmetry*, *Prog.Theor.Phys.* **70** (1983) 542.
- [13] G. L. Kane, C. F. Kolda, L. Roszkowski, and J. D. Wells, *Study of constrained minimal supersymmetry*, *Phys.Rev.* **D49** (1994) 6173–6210.
- [14] P. Bechtle, K. Desch, H. K. Dreiner, M. Kramer, B. O’Leary, *et. al.*, *What if the LHC does not find supersymmetry in the $\sqrt{s}=7$ TeV run?*, [1102.4693](#). * Temporary entry *.
- [15] S. Akula *et. al.*, *Interpreting the First CMS and ATLAS SUSY Results*, *Phys. Lett.* **B699** (2011) 377–382, [[1103.1197](#)].
- [16] M. J. Dolan, D. Grellscheid, J. Jaeckel, V. V. Khoze, and P. Richardson, *New Constraints on Gauge Mediation and Beyond from LHC SUSY Searches at 7 TeV*, *JHEP* **1106** (2011) 095, [[1104.0585](#)].
- [17] K. Sakurai and K. Takayama, *Constraint from recent ATLAS results to non-universal sfermion mass models and naturalness*, [1106.3794](#). * Temporary entry *.
- [18] T. Li, J. A. Maxin, D. V. Nanopoulos, and J. W. Walker, *Has SUSY Gone Undetected in 9-jet Events? A Ten-Fold Enhancement in the LHC Signal Efficiency*, [1108.5169](#).
- [19] S. Sekmen, S. Kraml, J. Lykken, F. Moortgat, S. Padhi, *et. al.*, *Interpreting LHC SUSY searches in the phenomenological MSSM*, [1109.5119](#). * Temporary entry *.
- [20] L. Randall and R. Sundrum, *Out of this world supersymmetry breaking*, *Nucl.Phys.* **B557** (1999) 79–118, [[hep-th/9810155](#)].
- [21] T. Gherghetta, G. F. Giudice, and J. D. Wells, *Phenomenological consequences of supersymmetry with anomaly induced masses*, *Nucl.Phys.* **B559** (1999) 27–47, [[hep-ph/9904378](#)].
- [22] J. L. Feng and T. Moroi, *Supernatural supersymmetry: Phenomenological implications of anomaly mediated supersymmetry breaking*, *Phys.Rev.* **D61** (2000) 095004, [[hep-ph/9907319](#)].
- [23] B. Allanach, G. Hiller, D. Jones, and P. Slavich, *Flavour Violation in Anomaly Mediated Supersymmetry Breaking*, *JHEP* **0904** (2009) 088, [[0902.4880](#)].
- [24] J. L. Feng, V. Rentala, and Z. Surujon, *WIMPless Dark Matter in Anomaly-Mediated Supersymmetry Breaking with Hidden QED*, [1108.4689](#).
- [25] J. L. Feng and Y. Shadmi, *WIMPless Dark Matter from Non-Abelian Hidden Sectors with Anomaly-Mediated Supersymmetry Breaking*, *Phys.Rev.* **D83** (2011) 095011, [[1102.0282](#)].
- [26] F. E. Paige and J. D. Wells, *Anomaly mediated SUSY breaking at the LHC*, [hep-ph/0001249](#).

- [27] A. Barr, C. Lester, M. A. Parker, B. Allanach, and P. Richardson, *Discovering anomaly mediated supersymmetry at the LHC*, *JHEP* **0303** (2003) 045, [[hep-ph/0208214](#)].
- [28] B. Allanach and M. J. Dolan, *Supersymmetry With Prejudice: Fitting the Wrong Model to LHC Data*, [1107.2856](#). * Temporary entry *.
- [29] I. Hinchliffe, F. E. Paige, M. D. Shapiro, J. Soderqvist, and W. Yao, *Precision SUSY measurements at CERN LHC*, *Phys. Rev.* **D55** (1997) 5520–5540, [[hep-ph/9610544](#)].
- [30] D. R. Tovey, *Measuring the SUSY mass scale at the LHC*, *Phys. Lett.* **B498** (2001) 1–10, [[hep-ph/0006276](#)].
- [31] B. C. Allanach, *SOFTSUSY: a program for calculating supersymmetric spectra*, *Comput. Phys. Commun.* **143** (2002) 305–331, [[hep-ph/0104145](#)].
- [32] P. Z. Skands, B. Allanach, H. Baer, C. Balazs, G. Belanger, *et. al.*, *SUSY Les Houches accord: Interfacing SUSY spectrum calculators, decay packages, and event generators*, *JHEP* **0407** (2004) 036, [[hep-ph/0311123](#)].
- [33] M. Bahr *et. al.*, *Herwig++ Physics and Manual*, *Eur. Phys. J.* **C58** (2008) 639–707, [[0803.0883](#)].
- [34] S. Ovin, X. Rouby, and V. Lemaitre, *DELPHES, a framework for fast simulation of a generic collider experiment*, [0903.2225](#).
- [35] M. Cacciari and G. P. Salam, *Jet clustering in particle physics, via a dynamic nearest neighbour graph implemented with CGAL*, *Unpublished* (2006).
- [36] M. Cacciari and G. P. Salam, *Dispelling the N^3 myth for the k_t jet-finder*, *Phys. Lett.* **B641** (2006) 57–61, [[hep-ph/0512210](#)].
- [37] W. Beenakker, R. Hopker, M. Spira, and P. M. Zerwas, *Squark and gluino production at hadron colliders*, *Nucl. Phys.* **B492** (1997) 51–103, [[hep-ph/9610490](#)].
- [38] F. E. Paige, S. D. Protopopescu, H. Baer, and X. Tata, *ISAJET 7.69: A Monte Carlo event generator for pp, anti-p p, and e+e- reactions*, [hep-ph/0312045](#).
- [39] B. Allanach, S. Kraml, and W. Porod, *Theoretical uncertainties in sparticle mass predictions from computational tools*, *JHEP* **0303** (2003) 016, [[hep-ph/0302102](#)].
- [40] C. Lester and D. Summers, *Measuring masses of semiinvisibly decaying particles pair produced at hadron colliders*, *Phys.Lett.* **B463** (1999) 99–103, [[hep-ph/9906349](#)].
- [41] A. Barr, C. Lester, and P. Stephens, *$m(T2)$: The Truth behind the glamour*, *J. Phys.* **G29** (2003) 2343–2363, [[hep-ph/0304226](#)].
- [42] H.-C. Cheng and Z. Han, *Minimal Kinematic Constraints and MT_2* , *JHEP* **12** (2008) 063, [[0810.5178](#)].
- [43] B. C. Allanach, A. J. Barr, A. Dabija, and C. Gwenlan, *Discovery reach for generic supersymmetry at the LHC: MT_2 versus missing transverse momentum selections for pMSSM searches*, *JHEP* **1107** (2011) 104, [[1105.1024](#)].
- [44] S. S. AbdusSalam *et. al.*, *Benchmark Models, Planes, Lines and Points for Future SUSY Searches at the LHC*, [1109.3859](#).
- [45] A. L. Read, *Modified frequentist analysis of search results (The $CL(s)$ method)*, . [CERN-OPEN-2000-205](#).
- [46] D. Alves, N. Arkani-Hamed, S. Arora, Y. Bai, M. Baumgart, *et. al.*, *Simplified Models for*

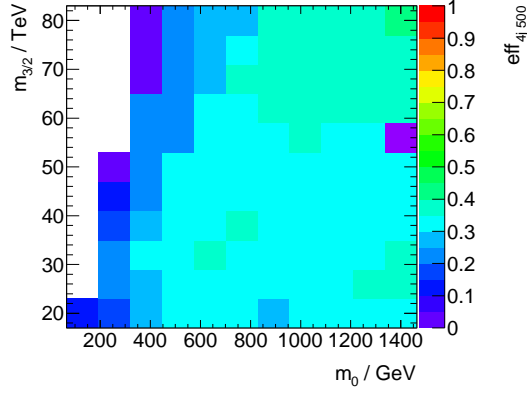
LHC New Physics Searches, [1105.2838](#). * Temporary entry *.



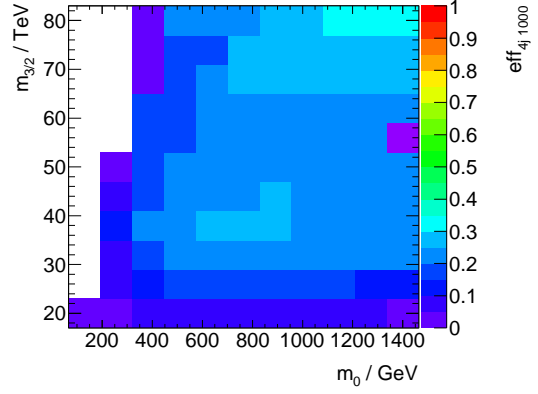
(a) 2 jets



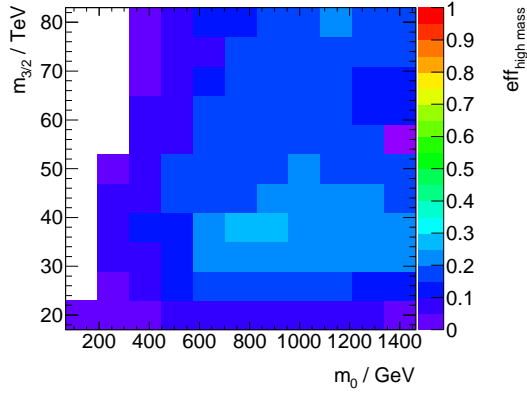
(b) 3 jets



(c) 4 jets

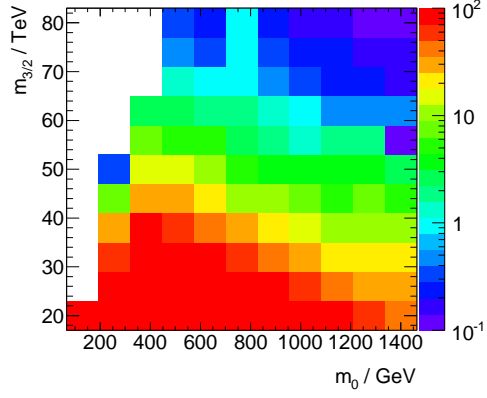


(d) 4 jets'

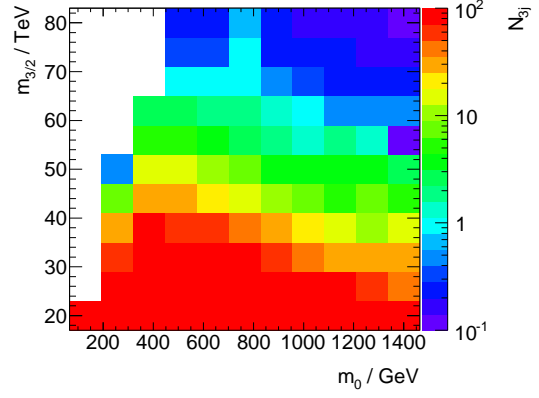


(e) high mass

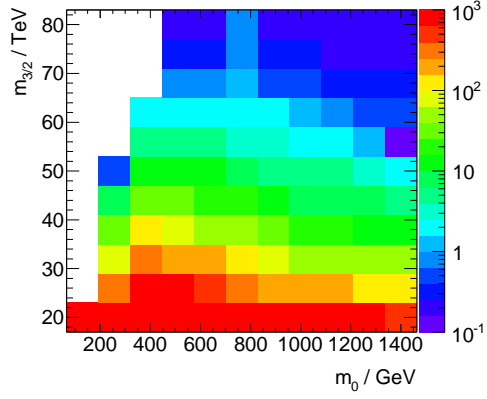
Figure 8. Efficiency of ATLAS signal selections in the mAMSB $m_0 - m_{3/2}$ plane. The flat correction factor for the missing calorimeter regions is not applied, as it adds no information about the physics of the signal models.



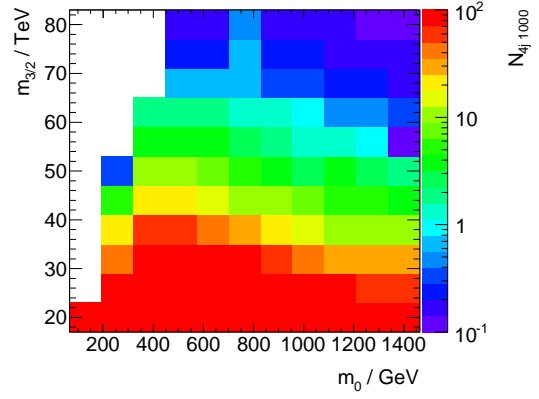
(a) 2 jets



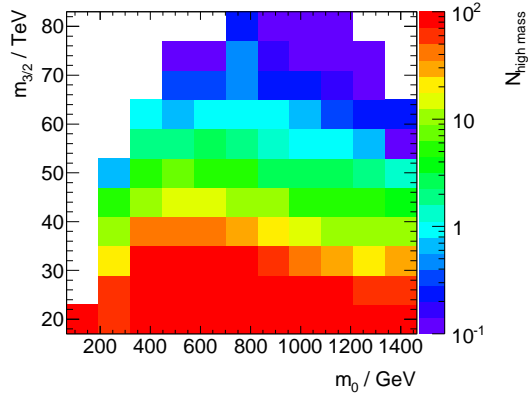
(b) 3 jets



(c) 4 jets



(d) 4 jets'



(e) high mass

Figure 9. Expected signal yield with 1.04 fb^{-1} of ATLAS signal selections in the mAMSB m_0 – $m_{3/2}$ parameter plane. White areas are either theoretically inconsistent, or have fewer than 0.1 expected signal events.

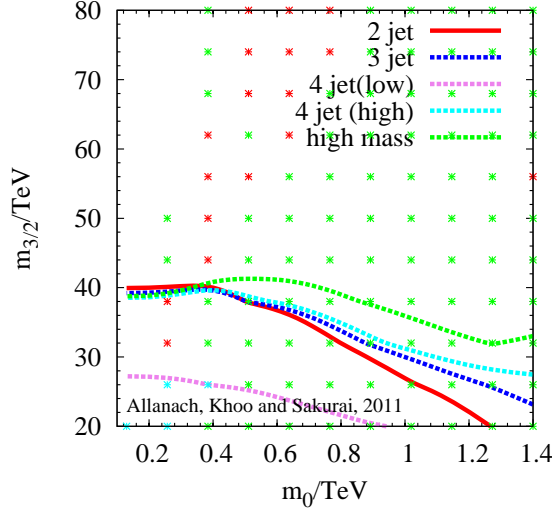


Figure 10. ATLAS mAMSB exclusion from the 1.04 fb^{-1} 0-lepton search, for $\tan\beta = 10$ and $\mu > 0$ for each signal region. The region under each line is excluded at the 95% confidence level for each individual signal region, labelled by the key and detailed in Table 1. The asterisks in the background display which signal region is expected to be the most sensitive at various points in parameter space. The white region in the upper left hand side of the plot is theoretically disfavoured due to the presence of negative mass squared sleptons (‘tachyons’).

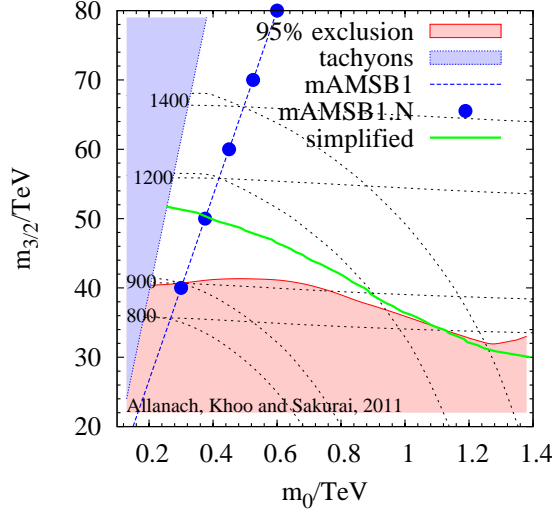


Figure 11. ATLAS mAMSB exclusion from the 1.04 fb^{-1} 0-lepton search, for $\tan\beta = 10$ and $\mu > 0$, with signal regions combined. The coloured region is excluded at the 95% confidence level. The black dashed lines show equal contours of gluino mass (almost horizontal lines) and squark mass (arcs) according to the label on the left-hand side of the figure, in units of GeV. We also show the benchmark mAMSB line and points defined in Ref. [44] and the simplified model approximation.